Materials Research Bulletin 47 (2012) 2288–2293

Contents lists available at SciVerse ScienceDirect

Materials Research Bulletin

journal homepage: www.elsevier.com/locate/matresbu

Structural and magnetic properties of pristine and Fe-doped NiO nanoparticles synthesized by the co-precipitation method

A.K. Mishra [a], S. Bandyopadhyay [b], D. Das [a,*]

[a] UGC-DAE Consortium for Scientific Research, Kolkata Centre, III/LB-8, Bidhannagar, Kolkata 70098, India
[b] Department of Physics, University College of Science, 92, A P C Road, Kolkata 700009, India

ARTICLE INFO

Article history:
Received 7 November 2011
Received in revised form 15 April 2012
Accepted 23 May 2012
Available online 19 June 2012

Keywords:
A. Nanostructures
A. Oxides
D. Magnetic properties

ABSTRACT

$Ni_{1-x}Fe_xO$ ($x = 0$ and 0.03) nanoparticles are synthesized by a chemical route. XRD and TEM measurements confirm phase purity and crystallinity of the nanoparticles. Fe substitution in NiO reduces considerably the average particle size of the nanoparticles. The pristine NiO sample with size 14 nm and Fe-substituted sample having size 7 nm show room temperature ferromagnetism. The pristine NiO having 31 nm size and Fe-substituted sample with size 25 nm are found to be antiferromagnetic. The M–H and M–T behavior of the pristine and Fe-doped samples are explained with a core–shell model with an antiferromagnetic core and a ferromagnetic shell. The disordered spins at the shell give rise to a spin-glass like frozen state below 10 K. The obtained room temperature ferromagnetism in the pristine and Fe-doped NiO has been attributed to particle size effect.

1. Introduction

Extensive research has been carried out recently on transition metal ion doped semiconductors because of their vast technological applications in magneto-electronic, opto-magneto-electronic and spintronic devices. There have been several reports on achieving room temperature ferromagnetism (RTFM) in different oxide based semiconducting materials such as SnO_2, ZnO and TiO_2 [1–8]. However the origin of RTFM in these oxides is still debated [9–11]. NiO is a widely investigated material because of its potential applications in different devices such as sensors, electrochromic displays and conducting electrodes [12,13]. NiO is a well known antiferromagnetic material with Neel temperature, $T_N = 523$ K. NiO essentially is an insulator with a band gap of nearly 4.0 eV but it also shows p-type semiconducting behavior due to either the presence of Ni^{2+} vacancies or when it is doped with other cations (e.g. Li $^{+}$) [14]. Kodama et al. had reported anomalous magnetic behavior like large magnetic moments, large coercivities and loop shifts at low temperatures in NiO nanoparticles (size 31.5 nm) that was explained by finite size effects [15]. Bi et al. reported ferromagnetic like behavior in ultrafine NiO nanocrystallites having grain size 5 nm. This behavior was ascribed to missing bonds and lattice distortion in the samples [16]. Winkler et al. suggested a core–shell model to describe ac-susceptibility results on 3 nm NiO nanoparticles [17]. Recently, there have been some reports in bulk and polycrystalline transition metal ion doped NiO. Wang et al. found RTFM in $Ni_{1-x}Fe_xO$ ($x = 0.02$) with a maximum magnetization of 0.575 emu g^{-1} at 10 kOe. They have ruled out the possibility of finite size effect for getting RTFM in their samples and suggested that ferromagnetic clusters formed due to compositional inhomogeneity might be responsible for the observed behavior [18]. Lin et al. reported RTFM in Fe-doped NiO nanopowder that was explained in terms of double exchange mechanism through the doped Fe ions and free charge carriers in the samples [14]. Douvalis et al. have investigated RTFM in 2% Fe^{57} doped NiO and have described its origin as due to the formation of a secondary phase like $NiFe_2O_4$ in the sample heat treated at 873 K whereas ferromagnetism in the sample heat treated at 673 K was assigned to finite size effect [19]. Recently, He et al. observed large room temperature ferromagnetism in $Ni_{1-x}Fe_xO$ ($x = 0$, 0.015, 0.03, 0.05 and 0.10) bulk samples [20]. The presence of an impurity phase like $NiFe_2O_4$ was described responsible for RTFM in all samples though the ferrite phase could not be detected by XRD in the samples with $x \leq 0.03$ due to being in trace amount. Manna et al. have shown room temperature ferromagnetism in Fe-doped NiO nanorod samples with a coercive field of 614 Oe [21]. A recent work by Raja et al. on polycrystalline Fe-doped NiO has reported ferromagnetic behavior at room temperature whereas the origin of ferromagnetism was proposed to be due to the formation of a secondary phase ($NiFe_2O_4$) in the samples [12]. Makhlouf et al. observed the absence of ferromagnetic behavior in the pristine NiO having particle size larger than 30 nm whereas ferromagnetism was observed at 296 K in the pristine NiO particles of size less than 8 nm. Most of the works carried out thereafter on Fe-doped NiO

* Corresponding author. Tel.: +91 33 2335 1866; fax: +91 33 2335 7008.
E-mail address: ddas@alpha.iuc.res.in (D. Das).

0025-5408/$ – see front matter © 2012 Elsevier Ltd. All rights reserved.
http://dx.doi.org/10.1016/j.materresbull.2012.05.046

were in bulk or polycrystalline form of particle size greater than 30 nm to avoid occurrence of ferromagnetism from pristine NiO component as reported by Makhlouf et al.

In the present work, structural and magnetic properties of pristine and 3% Fe-doped NiO nanoparticles prepared by a co-precipitation method are investigated. The particle sizes of the pristine samples are 14 nm and 31 nm (below and above the critical size of 30 nm as reported by Makhlouf et al.). After doping iron the above sizes are found to get reduced to 7 nm and 25 nm respectively. The structural and magnetic properties of the prepared nanomaterials are compared and discussed in the backdrop of the inconsistent results reported by previous workers as mentioned above. Structural and morphological studies were carried out by X-ray diffraction (XRD) and transmission electron microscopy (TEM) respectively. Magnetic measurements were done by a SQUID magnetometer. Room temperature ferromagnetism has been found in the pristine sample having size 14 nm whereas the pristine sample with size 31 nm showed antiferromagnetic behavior. The detailed M–H and M–T measurements indicate a core–shell type structure of the prepared samples. The disordered spins at the shell shows a "spin-glass" freezing below 10 K.

2. Experimental

Fe-doped NiO nanoparticles were prepared by a co-precipitation method followed by thermal treatment at relatively low temperature. Calculated amount of $NiCl_2{\cdot}4H_2O$ and $Fe(SO_4){\cdot}7H_2O$ were added into Milli-Q water. This solution was heated to 50 °C under vigorous stirring. Afterwards it was cooled down to room temperature and was hydrolyzed at a constant rate with drop wise addition of NaOH solution. The pH of the solution was maintained at 8. The obtained precipitate was washed several times with distilled water and absolute ethanol to remove possible ionic impurities. A similar method was used to prepare pristine NiO sample with required amount of $NiCl_2{\cdot}4H_2O$. The dried sample was heat treated at two different temperatures 400 and 700 °C in open atmosphere for 4 h to obtain the required nanomaterials of different grain sizes. Hence onward, the heat-treated pristine samples are described as N4 and N7 whereas Fe-substituted samples are marked as NF4 and NF7 corresponding to heat treatment at 400 and 700 °C respectively. The structure and phase purity of the prepared samples were characterized by a Bruker D8 Advance high-resolution X-ray diffractometer (HR-XRD) by using Cu Kα radiation of wavelength 1.54 Å. In addition to this, morphology and crystalline nature of the samples were checked by transmission electron microscopy (TEM). Selected area electron diffraction (SAED) and high-resolution transmission electron microscopy (HRTEM) tools were also used for further structural characterization. Magnetic properties were measured with a super conducting quantum interference device (SQUID) magnetometer (MPMS XL7, Quantum Design, USA).

3. Results and discussion

3.1. Structural analysis

Fig. 1 shows X-ray diffraction patterns of chemically synthesized nanomaterials. The calculated *d* values from the observed diffraction peaks were compared with the standard JCPDS data file, which confirms the formation of pure NiO phase in the samples. An additional peak of low intensity was detected in the XRD pattern of NF7 that was ascribed to a secondary $NiFe_2O_4$ phase. The ionic radii of Ni^{2+} and Fe^{3+}, are 0.69 and 0.64 Å respectively; therefore Ni^{2+} can be replaced in the lattice structure by Fe^{3+} ions. The average grain size of the samples was calculated by the Debye–Scherrer equation

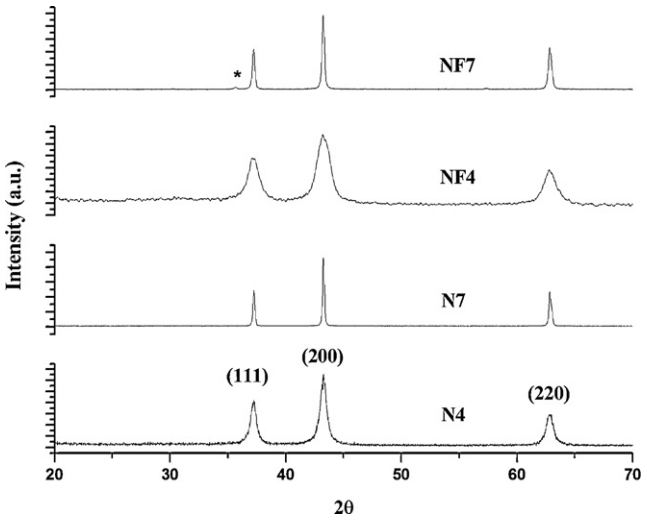

Fig. 1. X-ray diffractograms of the prepared $Ni_{1-x}Fe_xO$ (x = 0, 0.03) samples heat-treated at 400 and 700 °C. The mark (*) shows the impurity phase $NiFe_2O_4$ in NF7.

and was found to be 14, 7, 31 and 25 nm for N4, NF4, N7 and NF7 respectively. The drastically reduced grain size with Fe doping in the host matrix indicates restriction of host lattice growth on iron doping. The broadening and reduced intensity of peaks can be seen clearly in the case of Fe-doped NiO nanocrystalline samples. This is attributed to evolve strain in the matrix due to smaller particle size. A typical TEM picture of the pristine NiO nanostructures (sample N4) has been shown in Fig. 2(a). The estimated average particle sizes from TEM images have shown appreciable agreement with XRD results. A change in morphology is found with insertion of dopant Fe atoms in the host NiO matrix. As can be seen from Fig. 2(b), shape of the particles in the Fe-doped sample has transformed to nearly rod-like shape from being spherical in the pristine sample. High-resolution transmission electron microscopy (HRTEM) was carried out to check the crystallinity and phase purity of the samples. Clear fringes have been observed (Fig. 2(c)) in HRTEM image of the sample N4 indicating high crystallinity and nearly defect-free nature of the sample. The interplanar distance between adjacent planes is obtained as 2.09 Å, which corresponds to (2 0 0) plane of NiO structure. The selected area electron diffraction (SAED) pattern of the same sample has been displayed in the inset of Fig. 2(a) and (b). The observed rings are identified as that of NiO, which confirms crystalline nature and phase purity of the prepared samples.

3.2. Magnetization studies

Magnetization (M) of the samples measured as a function of temperature (T) in zero-field-cooled (ZFC) and field-cooled (FC) conditions with an applied field of 100 Oe have been displayed in Fig. 3. The ZFC curves of the pristine NiO (N4) and Fe-substituted NiO (NF4) show two peaks. The broad peaks observed at 90 K and 140 K in the samples N4 and NF4 respectively are assigned to gradual superparamagnetic blocking of the relaxing spin moments essentially at the core of the particles with reduction of temperature. The broadening of the peaks is caused by distribution of particle size in the samples that results in distribution of anisotropy energy barrier. The sharp peaks observed around 12 K and 8 K in N4 and NF4 respectively are attributed to freezing of the surface magnetic moments of the nanoparticles at low temperature giving rise to the formation of "spin-glass" like state. The bifurcation of the ZFC and FC curves observed in the samples N4 and NF4 at 225 and 270 K respectively also indicates the presence of relaxing spin moments in the samples. The TEM pictures of the

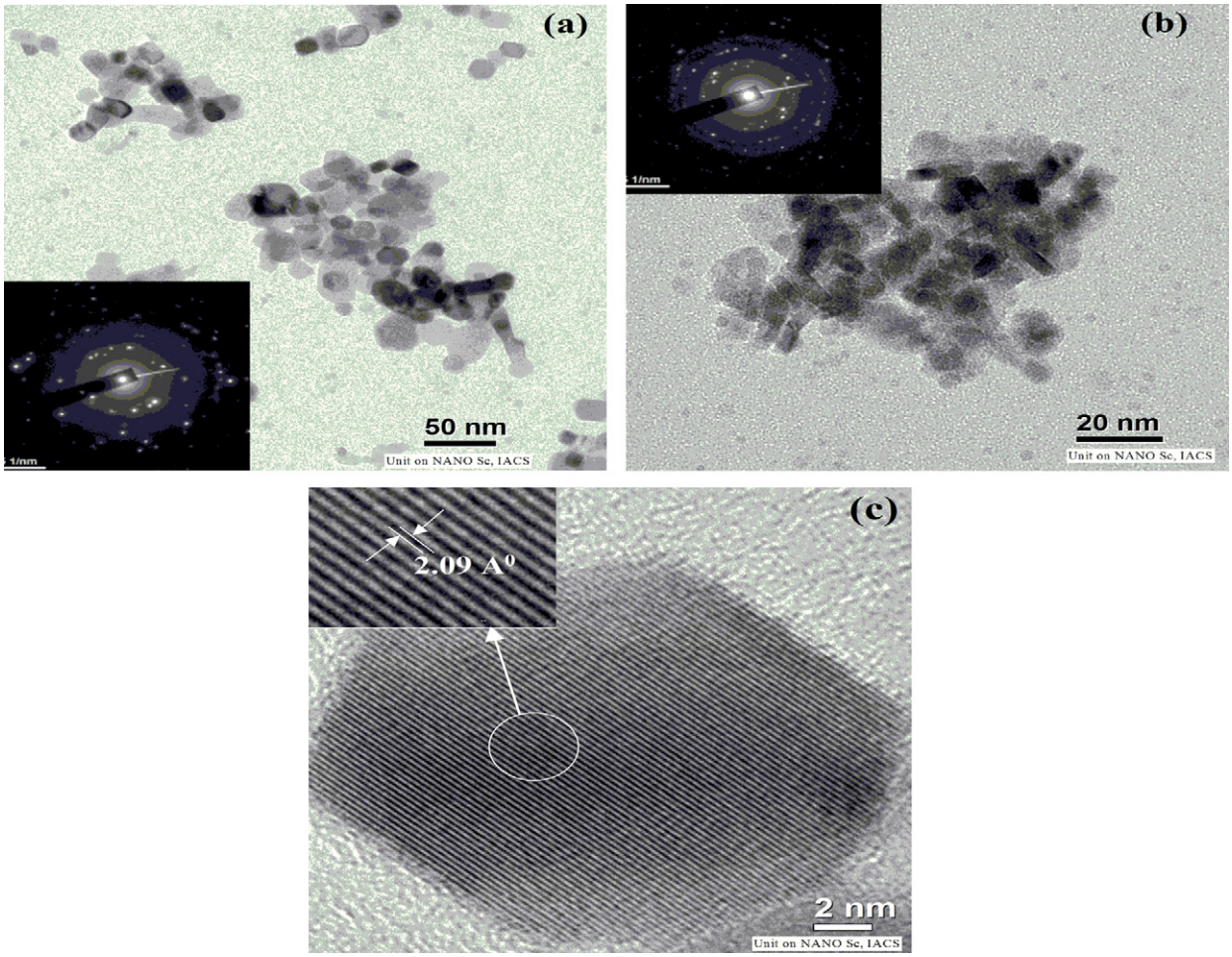

Fig. 2. TEM image of (a) N4, (b) NF4 and insets show SAED patterns of the same sample, and (c) high-resolution TEM image of N4 sample.

prepared nanoparticles also support the existence of a distribution of particle size. The observed variation of magnetization with temperature as discussed above can be explained with a core–shell type structure of the nanoparticles. The uncompensated spin in the core structure is responsible for the superparamagnetic behavior characterized by broad peaks in the zero-field-cooled M–T curves. The disordered spins at the shell near the surface are responsible for the observed spin-glass like freezing at lower temperatures. Similar core–shell structure has been reported recently in pristine NiO nanoparticles by others also though particle size was rather low in their study [17]. It is also to be noticed that NF4 shows higher average blocking temperature than that shown by N4, though NF4 has lower particle size in comparison to N4. This unusual behavior indicates the presence of interparticle interaction among the particles that may increase the average blocking temperature. Shifting of blocking temperature due to interparticle interaction has been reported in some other systems also [23,24]. For more precise information about interparticle interaction in samples N4 and NF4, ac-susceptibility measurements were carried out. The obtained results are shown in Fig. 4. Both the samples show similar behavior as was found for dc magnetization measurements (Fig. 3). The peak observed at lower temperature did not show any shift with varied frequencies. In the case of the sample N4, the other broad peak observed at higher temperature has shown small shift of peak position with frequency. For noninteracting superparamagnetic (SPM) particles, T_b shows substantial frequency dependence while frequency dependence of T_b is less prominent for spin-glass (SG) or interacting SPM particles. A useful parameter that represents relative shift of the blocking temperature per a frequency decade is given by

$$\Phi = \frac{\Delta T}{T_b \Delta \log_{10} f} \tag{1}$$

where ΔT_b is the difference between the blocking temperature measured in $\Delta \log_{10} f$ and f is the ac magnetic field frequency [25]. The values of this parameter are in the range 0.1–0.13 for non-interacting superparamagnetic particles whereas for magnetically interacting as well as for spin-glass, the values of the parameter Φ are observed in the range 0.05–0.005. The obtained value of the parameter Φ for N4 is 0.05. This value suggests the presence of weak interparticle interaction in the sample. For NF4, the value of T_b has been observed to be 150 K that is clearly higher than that in N4. Similar observation has also been noticed in dc magnetic behavior of N4 and NF4. The ac-susceptibility measurement of NF4 did not show notable shift of T_b with varied frequency. This is assigned to increased interparticle interaction in the sample NF4. This can be explained by the fact that the number of particles per unit volume increases when particle size decreases thus the average distance between the particles also decreases [26].

Fig. 5 shows M–H curves of the samples N4 and NF4 recorded at room temperature. Both the curves show an open loop in the low field (less than 1 T) region superposed on a more or less linear behavior in the high field region. The observed M–H curves can be explained by taking into account the core–shell configuration of the nanoparticles as proposed by Winkler et al. [17]. The open

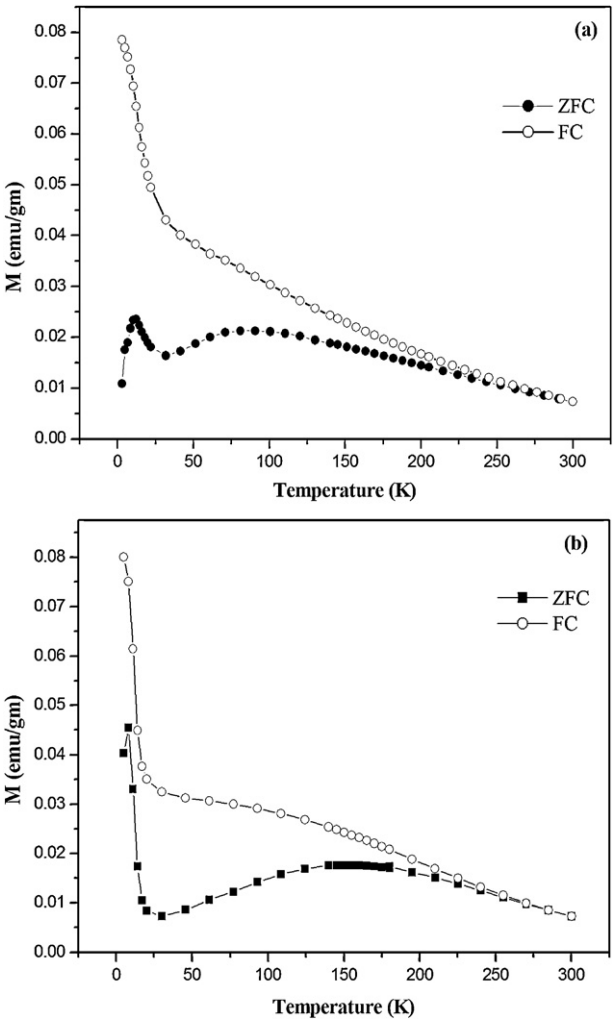

Fig. 3. Magnetization vs temperature curve of (a) N4 and (b) NF4.

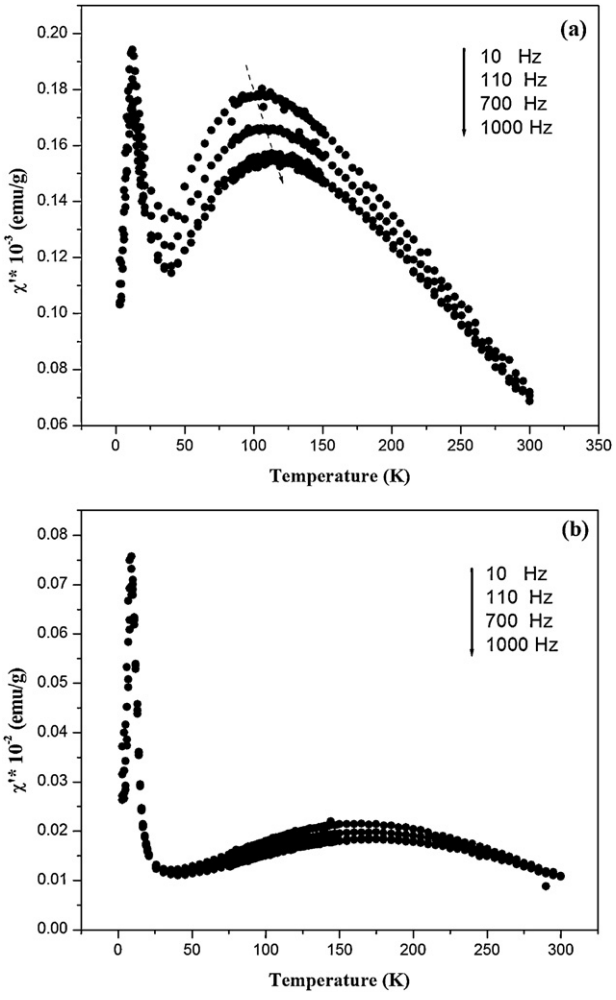

Fig. 4. Temperature dependent curve of χ' for (a) N4 and (b) NF4.

loops seen in the low field region are due to uncompensated spins at the core of the nanoparticles that tend to get aligned towards the applied field whereas the linear parts at higher magnetic field corresponds to spins at the surface of the materials that remain in the disordered state at room temperature even after application of the magnetic field.

The coercivity and remanent magnetization values obtained from the loops are 80 Oe and 0.072 emu g^{-1} respectively for the sample N4 whereas for NF4 sample the values are 20 Oe and 0.015 emu g^{-1} respectively. The finite values of coercivity and remanent magnetization found for N4 and NF4 shows presence of room temperature ferromagnetism in these two samples. The low value of coercivity found in NF4 is assigned to smaller particle size of the sample. It is also clear from Fig. 5 that magnetization value at a particular field is more in the sample NF4 compared to that in the sample N4. Doping of Fe in NiO matrix creates extra charge carriers that generate double exchange interaction as has been reported by others [14,21]. Apart from double exchange interaction, interparticle interaction is also present in Fe doped NiO sample. Both these factors will increase the effective magnetic moment of the particles in NF4.

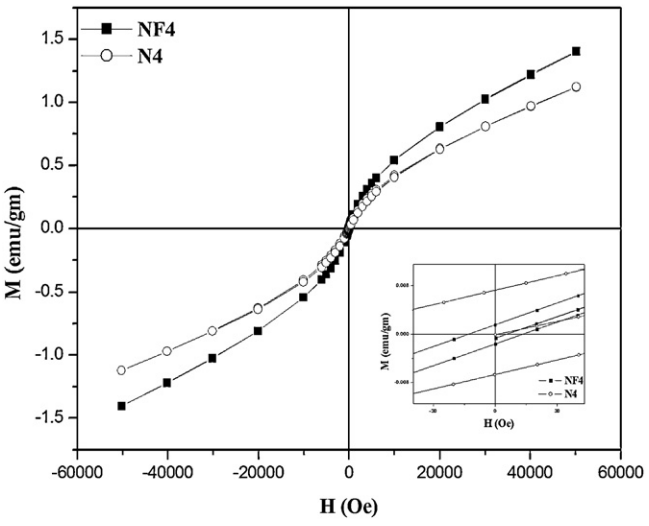

Fig. 5. Room temperature M–H loops of N4 and NF4 sample.

Fig. 6 shows M–H loops of the samples N7 and NF7 recorded at room temperature. The sample N7 shows a typical linear behavior expected for an antiferromagnetic material. It is to be noted that average particle size of this sample 31 nm. The absence of ferromagnetism in this sample in contrast to N4 having average particle size 14 nm supports the results obtained by Makhlouf et al. [22]. The sample NF7 shows a drastically different behavior from that seen in N7. A clear loop is seen which tends to saturate in the high field region. The coercive field obtained from the loop is ~400 Oe, much higher than that found for the sample NF4. This is

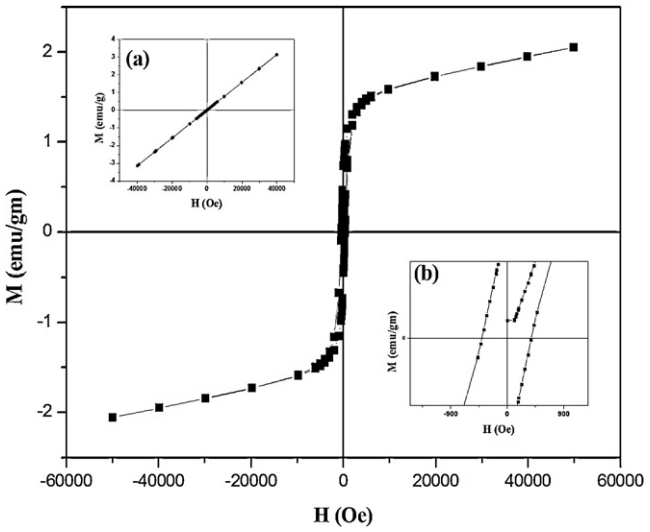

Fig. 6. Room temperature M–H loop of NF7. Inset (a) shows room temperature M–H loop of N7 and (b) shows enlarged central part of NF7.

attributed to the presence of $NiFe_2O_4$ phase as an impurity in the sample NF7. The existence of $NiFe_2O_4$ in the sample NF7 which was heat-treated at 700 °C has also been confirmed by XRD measurements. In order to get further information, hysteresis measurements were carried out at lower temperatures under the zero-field-cooled (ZFC) and field-cooled (FC) conditions. The M–H loops recorded in the ZFC condition at lower temperature were open up to ~2 T field in contrast with the loops recorded at room temperature which were open up to ~1 T. The variation of coercive field with temperature in ZFC condition for the sample N4 and NF4 are shown in Fig. 7. The coercive field increases steadily for both the samples with reduction of temperature. The sharp rise in H_c at lower temperatures in both the samples is attributed to the freezing of surface spins at lower temperature as has been inferred from the M–T data discussed earlier [27]. The field-cooled M–H measurements at 30 K in an applied field of 30 kOe were carried out on the samples N4, NF4 and NF7 and the coercivity found are 816, 673 and 709 Oe respectively. The increase of coercivity at low temperature particularly for the samples N4 and NF4 can be explained as due to the interaction between surface and core spin and the tendency of the surface spins to get frozen as the temperature of the system is lowered.

The FC measurements also show loop shifts in negative field direction for the samples N4 and NF7 indicating presence of exchange bias in these samples. The higher exchange bias seen in the sample NF7 is assigned to the presence on ferrimagnetic impurity phase ($NiFe_2O_4$) in the sample. Fig. 7 also shows variation of remanent magnetization with temperature for the samples N4 and NF4. The trend for both the samples is similar, M_r increases with decrease of temperature. Hysteresis measurements of the sample N4 and NF4 were also performed at 6 K after cooling the samples from room temperature in the presence of 30 kOe field. Fig. 8 shows the loops for the samples N4 and NF4 in ZFC and FC conditions recorded at 6 K. A clear vertical shift of the FC loop with respect to the ZFC loop is seen in both the samples (more

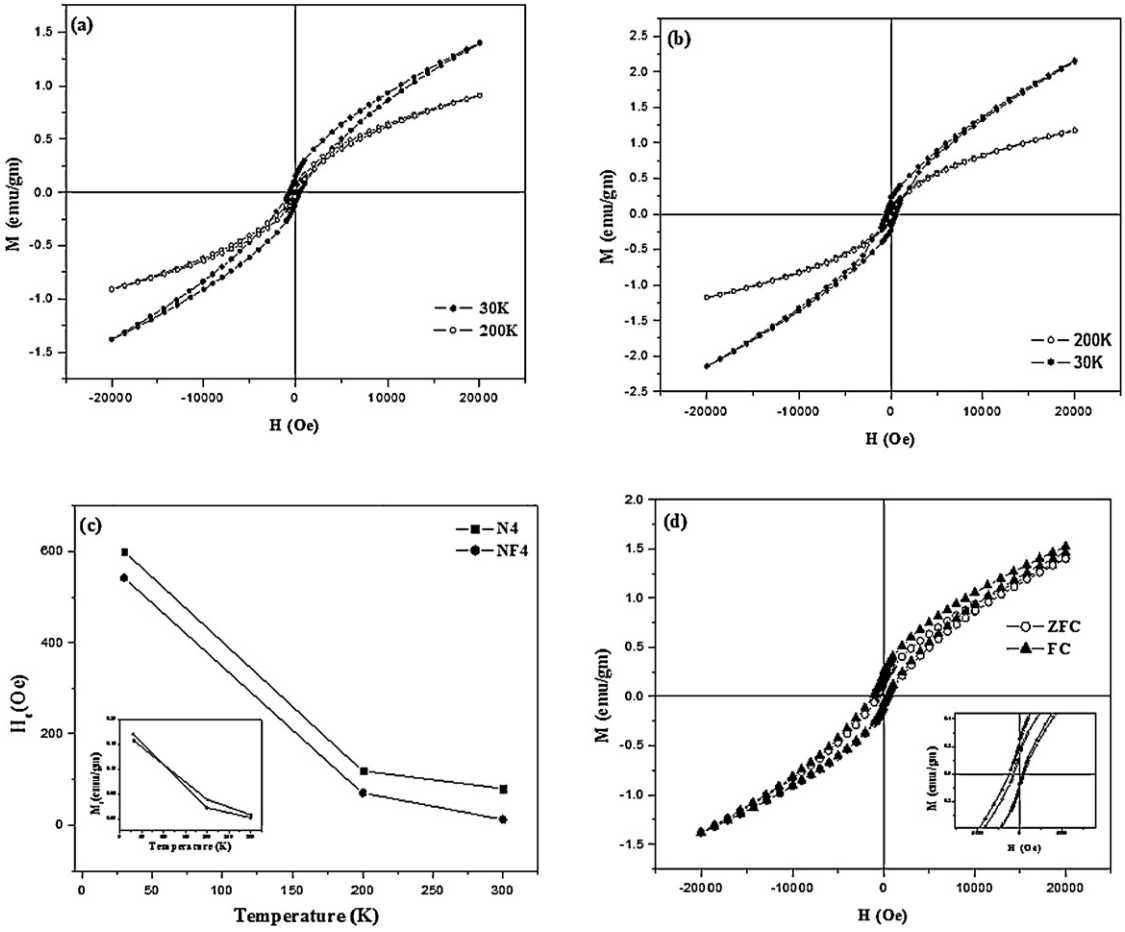

Fig. 7. M–H loops at 30 K and 200 K of (a) N4 and (b) NF4. (c) The variation of H_c and M_r with temperature, and (d) the exchange bias effect in N4 sample at 30 K.

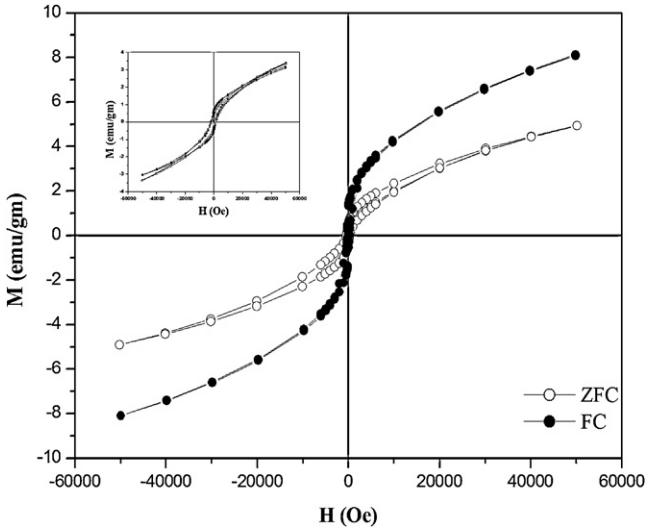

Fig. 8. ZFC-FC hysteresis loop at 6 K for NF4 and inset shows the same measurement for N4 at 6 K.

prominent in the case of NF4). This vertical shift is attributed to freezing of surface spin in the direction of applied field [28]. The spin-glass like behavior as described above is most likely to be due to broken bonds and disorder in the materials as their grain size is reduced to nanometric dimension [15]. Thus the room temperature ferromagnetism seen in the sample N4 and NF4 is essentially coming from the particle size effect. The nearly saturated M–H loop observed at room temperature for the sample NF7 and the corresponding large coercivity is attributed to the presence of $NiFe_2O_4$ impurity phase in the sample. The impurity phase has resulted as the sample was heat treated at 700 °C.

4. Conclusion

Pristine and Fe-substituted NiO nanoparticles with high crystallinity were prepared by a chemical route. The M–H and M–T behavior of the samples could be explained with a core–shell model. The open loops seen in M–H curves are due to the uncompensated spins at the core whereas the surface spins in the shell gives a linear M–H behavior. Exchange bias and vertical loop shifts that are found to be more prominent at lower temperature also point to the existence of core shell structure. The surface disorder or vacancies gave rise to spin-glass like freezing of magnetic moments below 10 K.

Acknowledgment

One of the authors (A.K. Mishra) thanks CSIR, Govt. of India for the award of senior research fellowship.

References

[1] H. Ohno, Science 281 (1998) 951.
[2] K. Sato, H. Katayama-Yoshida, Semicond. Sci. Technol. 17 (2002) 367.
[3] T. Dietl, H. Ohno, F. Matsukura, J. Cibert, D. Ferrand, Science 287 (2000) 1019.
[4] K. Ueda, H. Tabata, T. Kawai, Appl. Phys. Lett. 79 (2001) 988.
[5] S. Ramchandran, A. Tiwari, J. Narayan, Appl. Phys. Lett. 84 (2004) 5255.
[6] J.M.D. Coey, A.P. Douvails, C.B. Fitzgerald, M. Venkatesan, Appl. Phys. Lett. 84 (2004) 1332.
[7] A.K. Mishra, T.P. Sinha, S. Bandyopadhyay, D. Das, Mater. Chem. Phys. 125 (2011) 252.
[8] Y. Matsumoto, M. Murakami, T. Shono, T. Hasegawa, T. Fukumara, M. Kawasaki, P. Ahmet, T. Chikyou, S. Koshihara, H. Koinuma, Science 291 (2001) 854.
[9] S. Kolesnisk, B. Dabrowski, J. Appl. Phys. 96 (2004) 5379.
[10] A.S. Risbud, N.A. Spalidin, Z.Q. Chen, S. Stemmer, R. seshadri, Phys. Rev. B 68 (2003) 205202.
[11] J.H. Kim, H. Kim, D. Kim, Y.E. Ihm, W.K. Choo, J. Appl. Phys. 92 (2002) 6066.
[12] S.P. Raja, C. Venkateswaran, J. Phys. D: Appl. Phys. 42 (2009) 145001.
[13] J.B. Wu, J. Nan, C.W. Nan, Y. Lin, Y. Deng, S. Zhao, Mater. Sci. Eng. B 99 (2003) 294.
[14] Y.H. Lin, J. Wang, J. Cai, M. Ying, R. Zhao, M. Li, C.W. Nan, Phys. Rev. B 73 (2006) 193308.
[15] R.H. Kodama, S.A. Makhlouf, A.E. Berkowitz, Phys. Rev. Lett. 79 (1997) 1393.
[16] H. Bi, S. Li, Y. Zhang, Y. Du, J. Magn. Magn. Mater. 277 (2004) 363.
[17] E. Winkler, R.D. Zysler, M.V. Mansilla, K.N. Trohidou, Nanotechnology 19 (2008) 185702.
[18] J. Wang, J. Cai, Y.H. Lin, C.W. Nan, Appl. Phys. Lett. 87 (2005) 202501.
[19] A.P. Douvalis, L. Jankovic, T. Bakas, J. Phys.: Condens. Matter 19 (2007) 436203.
[20] J.H. He, S.L. Yuan, Y.S. Yin, Z.M. Tian, P. Li, Y.Q. Wang, K.L. Liu, C.H. Wang, J. Appl. Phys. 103 (2008) 023906.
[21] S. Manna, A.K. Deb, J. Jagannath, S.K. De, J. Phys. Chem. C 112 (2008) 10659.
[22] S.A. Makhlouf, F.T. Parker, F.E. Spada, A.E. Berkowitz, J. Appl. Phys. 81 (1997) 5561.
[23] J. Dai, J.Q. Wang, C. Sangregorio, J. Fang, E. Carpenter, J. Tang, J. Appl. Phys. 87 (2000) 7397.
[24] C.R. Vestal, Q. Song, Z. John Zhang, J. Phys. Chem. B 108 (2004) 18222.
[25] G.F. Goya, V. Sagredo, Phys. Rev. B 64 (2001) 235208.
[26] A.K. Pramanik, A. Banerjee, Phys. Rev. B 82 (2010) 094402.
[27] E. Winkler, R.D. Zysler, M.V. Mansilla, D. Fiorani, Phys. Rev. B 72 (2005) 132409.
[28] S. Mandal, S. Banerjee, K.S.R. Menon, Phys. Rev. B 80 (2009) 214420.